



RESEARCH ARTICLE

10.1029/2018JD028356

Key Points:

- Nonspherical hydrometeors and anisotropic diffusional growth can influence collisional charge separation
- The importance of local diffusional graupel growth can be masked by ice multiplication
- Interpretation and application of traditional RDGR plots are complicated by strong hydrometeor size and shape sensitivities

Correspondence to:

F. Glassmeier,
Franziska.Glassmeier@noaa.gov

Citation:

Glassmeier, F., Arnold, L., Dietlicher, R., Paukert, M., & Lohmann, U. (2018). A modeling study on the sensitivities of atmospheric charge separation according to the relative diffusional growth rate theory to nonspherical hydrometeors and cloud microphysics. *Journal of Geophysical Research: Atmospheres*, 123, 12,236–12,252. <https://doi.org/10.1029/2018JD028356>

Received 27 JAN 2018

Accepted 6 SEP 2018

Accepted article online 22 SEP 2018

Published online 9 NOV 2018

©2018. The Authors.

This is an open access article under the terms of the Creative Commons Attribution-NonCommercial-NoDerivs License, which permits use and distribution in any medium, provided the original work is properly cited, the use is non-commercial and no modifications or adaptations are made.

A Modeling Study on the Sensitivities of Atmospheric Charge Separation According to the Relative Diffusional Growth Rate Theory to Nonspherical Hydrometeors and Cloud Microphysics

F. Glassmeier¹ , L. Arnold¹, R. Dietlicher¹ , M. Paukert² , and U. Lohmann¹

¹Institute for Atmospheric and Climate Science, ETH Zurich, Zurich, Switzerland, ²Institute of Meteorology and Climate Research—Atmospheric Aerosol Research, Karlsruhe Institute of Technology, Karlsruhe, Germany

Abstract Collisional charge transfer between graupel and ice crystals in the presence of cloud droplets is considered the dominant mechanism for charge separation in thunderclouds. According to the relative diffusional growth rate (RDGR) theory, the hydrometeor with the faster diffusional radius growth is charged positively in such collisions. We explore sensitivities of the RDGR theory to nonspherical hydrometeors and six parameters (pressure, temperature, liquid water content, sizes of ice crystals, graupel, and cloud droplets). Idealized simulations of a thundercloud with two-moment cloud microphysics provide a realistic sampling of the parameter space. Nonsphericity and anisotropic diffusional growth strongly control the extent of positive graupel charging. We suggest a tuning parameter to account for anisotropic effects not represented in bulk microphysics schemes. In a susceptibility analysis that uses automated differentiation, we identify ice crystal size as most important RDGR parameter, followed by graupel size. Simulated average ice crystal size varies with temperature due to ice multiplication and heterogeneous freezing of droplets. Cloud microphysics and ice crystal size thus indirectly determine the structure of charge reversal lines in the traditional temperature–water–content representation. Accounting for the variability of ice crystal size and potentially habit with temperature may help to explain laboratory results and seems crucial for RDGR parameterizations in numerical models. We find that the contribution of local water vapor from evaporating rime droplets to diffusional graupel growth is only important for high effective water content. In this regime, droplet size and pressure are the dominant RDGR parameters. Otherwise, the effect of local graupel growth is masked by small ice crystal sizes that result from ice multiplication.

1. Introduction

Theories for the electrification of thunderclouds have been proposed for more than a hundred years. The basic characteristics of most of these theories are summarized in Table 1. They suggest the generation of oppositely charged hydrometeors of different terminal velocities (Table 1, *resulting charging*), either due to rebounding collisions between different types or sizes of hydrometeors or due to the breakup of a single particle (Table 1, *feature*). Before the collision or breakup event, positive and negative charges are usually distributed heterogeneously within at least one of the involved hydrometeors—which does not yet carry a net charge—due to various mechanisms (Table 1, *driving factor*). After collision and charge transfer of positive or negative charges (Table 1, *transfer*) or breakup, the net and oppositely charged particles are gravitationally separated. This leads to net charged regions within a thundercloud, although positive and negative charges exist everywhere in a cloud (Takahashi et al., 1999).

It is now widely agreed that opposite charging of graupel particles and ice crystals during their rebounding collisions in the mixed phase zone of thunderclouds is required for significant thundercloud electrification. The consensus for the importance of this noninductive mechanism of rime electrification is supported by numerical models (e.g., Helsdon et al., 2001; Mansell et al., 2010) and field observations in which regions of high electrification were found to correlate with the presence of graupel, ice crystals, and supercooled cloud droplets (e.g., Latham & Dye, 1989; Latham et al., 2007; Reinhart, 2014). Field measurements of Takahashi et al. (1999) identified graupel and ice crystals as main carriers of charge, often showing opposite charges of approximately the same magnitude. Furthermore, laboratory studies showed that in the presence of cloud

Table 1
Characteristics of Charge Generation Theories Due to Particle-Breakup (b) and/or Collision Between Particles (c)

Theory	Feature	Driving factor	Transfer ^a	Resulting charging	Issues
Inductive theories (Matthews & Mason, 1964; Sartor, 1954; Wilson, 1929)	b or c	polarized particles	electrons ^b	depending on the theory	cannot explain some field observations (Christian et al., 1980; Latham & Dye, 1989); insignificant in laboratory studies (Gaskell, 1981); insufficient for initial electrification (Latham & Dye, 1989; Latham et al., 2007) but may be a relevant secondary mechanism (Brooks & Saunders, 1994)
Noninductive droplet breakup (Simpson, 1909, 1927; Zlich et al., 2008)	b	electrical double layer	—	large/small droplets: + or —	only explains lower half of typical tripole
Charging during melting (Dinger & Gunn, 1946)	b	electrical double layer	—	melting ice particles: +, small droplets: —	
Splintering during droplet freezing (Kolomeychuk et al., 1975; Latham & Mason, 1961b)	b	temperature gradients	—	ice splinters: +, graupel/droplets: —	possibly unimportant (Pruppacher & Klett, 2010); only explains upper half of typical tripole
Workman-Reynolds effect (Workman & Reynolds, 1950)	b + c	chemical components	—	graupel/droplets: + or —	inconsistent with some laboratory observations (Latham & Warwicker, 1980); only explains either upper or lower dipole
Ionic mechanism (Jungwirth et al., 2005)	c	chemical components	ions	graupel/ice: + or —	cannot explain observed charge generation with pure water and ice (Reynolds et al., 1957); minor effect of contaminants (Latham & Mason, 1961a); only explains either upper or lower dipole
Thermoelectric effect (Latham & Mason, 1961a; Reynolds et al., 1957)	c	temperature gradients	protons	graupel/ice: + or —	small generated charge (Pruppacher & Klett, 2010); inconsistent with some laboratory observations (Gaskell & Illingworth, 1980)
temperature gradient within frost fibers (Caranti et al., 1991)	b + c	temperature gradients	—	graupel/ice: + or —	inconsistent with some laboratory observations (Jayaratne, 1991; Marshall et al., 1978; Saunders et al., 2001); significant charge separation is also observed without fracturing (Avila et al., 1995)
Contact potential (Buser & Aufdermaur, 1977; Marshall et al., 1978)	c	surface potential	electrons	graupel/ice: + or —	inconsistent with some laboratory observations (Caranti & Illingworth, 1980; Jayaratne et al., 1983)
Dislocation (Keith & Saunders, 1990)	c	structural defects	protons	graupel/ice: + or —	inconsistent with some laboratory observations (Saunders et al., 2001); inefficient in combination with collisional melting or radial temperature gradient theories
Relative diffusional growth rate (Baker et al., 1987)	c	diffusional growth rate	not specified	graupel/ice: + or —	inconsistent with some laboratory observations (Keith & Saunders, 1990); fraction of graupel surface influenced by the local water vapor field is small (Williams et al., 1991)
Quasi-liquid layer (Baker & Dash, 1989)	c	electrical double layer	negative ions	graupel/ice: + or —	inconsistent with some laboratory observations (Mason & Dash, 2000)
Radial temperature gradient (Saunders et al., 1991)	c	temperature gradients	negative ions	graupel/ice: + or —	argued to be unimportant (Jayaratne, 1993); only explains lower dipole
Collisional melting (Dash et al., 2001)(Dash & Wettlaufer, 2003)	c	structural defects	negative ions	graupel/ice: + or —	suggest transfer of hydroxide ions that would be compensated by proton transfer suggested by the dislocation theory

^aNo charge is transferred for breakup theories. ^bOnly for the inductive theories that depend on the charge generation during collisions of hydrometeors (Sartor, 1954).

droplets sufficient charge for thundercloud electrification can be generated on graupel and ice crystals during their rebounding collision (e.g., Baker et al., 1987; Jayaratne et al., 1983; Keith & Saunders, 1990; Marshall et al., 1978; Reynolds et al., 1957; Takahashi, 1978). Following previous literature, only the sign of graupel charge will be indicated in the following while the ice crystals are implicitly assumed to be charged oppositely.

Observations show a quadrupolar charge structure in the main updraft regions of thunderstorms (Stolzenburg et al., 1998a). Due to its requirement of mixed-phase microphysical conditions, charge separation by graupel-ice crystal collision can explain the dominant lower tripole of this charge structure if the main negative charge center coincides with a reversal of graupel charge separation from a net negative charge transfer to the graupel particles in higher regions of the cloud and net positive charge transfer below. Then, net negative charge must converge in the region of charge transfer reversal since the net charges on both the graupel particles falling in from above and ice crystals lifted from below are negative. The sign of charge (SoC) reversal occurs between -10 and -20 °C (Williams, 1989), where lower temperatures are expected for deeper storms (Stolzenburg et al., 1998a).

Laboratory studies found that in general temperatures below -10 to -15 °C and low to moderate effective water content (EW) lead to a net negative graupel charge transfer and vice versa (Jayaratne et al., 1983; Keith & Saunders, 1990; Saunders & Peck, 1998; Saunders et al., 2001, 1991). The EW is the product of liquid water content (LWC) and the collision efficiency between cloud droplets and graupel particles and thus a measure of water that is available for riming. As LWC and temperature generally decrease with height within a thundercloud, those studies support the theory of the main tripolar charge distribution by gravitational sorting of ice crystals and graupel particles. Numerical studies showed that parameterizations based on such laboratory results are indeed able to produce realistic charge structures in thunderclouds (e.g., Barthe et al., 2005; Mansell et al., 2010; Scavuzzi & Caranti, 1996).

A good candidate to describe the SoC separation from graupel-ice crystal collisions is the relative diffusional growth rate (RDGR) theory (Baker et al., 1987; Mitzeva et al., 2005). According to this theory, the crucial factor for the SoC separation is the diffusional radius growth rate of the particles, dr/dt . The particle that grows faster by vapor diffusion is charged positively during collisions and vice versa. The theory assumes that droplets involved in the riming of a graupel particle partially evaporate while they freeze onto its surface and thus provide a local source of water vapor. This vapor from the local field is thought to be important, as it provides an additional vapor source to the graupel particle only, thus favoring positive graupel charging by faster diffusional growth. The graupel is assumed to grow from the ambient vapor field (here also called far field) with a rate $(dr_g/dt)_{far}$ and from the local vapor field with a rate $(dr_g/dt)_{loc}$ while the ice crystal grows from the ambient vapor alone with a rate dr_i/dt as illustrated in Figure 1. The RDGR theory does not specify the mechanism of charge transfer between a graupel and ice crystal during their rebounding collision. According to Baker et al. (1987) any process that is influenced by the diffusional growth rate could be responsible for the collisional generation of charged graupel particles and ice crystals.

To summarize, the SoC obtained by the graupel particle is determined by

$$\text{SoC} = \text{sign}(\Delta) \quad (1)$$

$$\Delta = \left(\frac{dr_g}{dt} \right)_{far} + \left(\frac{dr_g}{dt} \right)_{loc} - \frac{dr_i}{dt} \quad (2)$$

$$= \frac{\partial r_g}{\partial m_g} \left[\left(\frac{dm_g}{dt} \right)_{far} + \left(\frac{dm_g}{dt} \right)_{loc} \right] - \frac{\partial r_i}{\partial m_i} \frac{dm_i}{dt}, \quad (3)$$

where the diffusional growth of hydrometeors is described in the form of mass growth rates dm/dr that are converted into radius growth rates. For this conversion, previous studies have assumed a spherical mass-radius relationship of $m(r) = \rho \frac{4}{3} \pi r^3$ with density ρ .

While the RDGR theory has been qualitatively supported by laboratory observations (Emersic & Saunders, 2010), a quantitative confirmation is missing so far. The reason for this probably lies in the complex sensitivities of the theory, which have been explored in theoretical studies (Mitzeva et al., 2005; Tsenova et al., 2009). The RDGR theory requires a variety of input parameters such as temperature, pressure, LWC, supersaturation, sizes

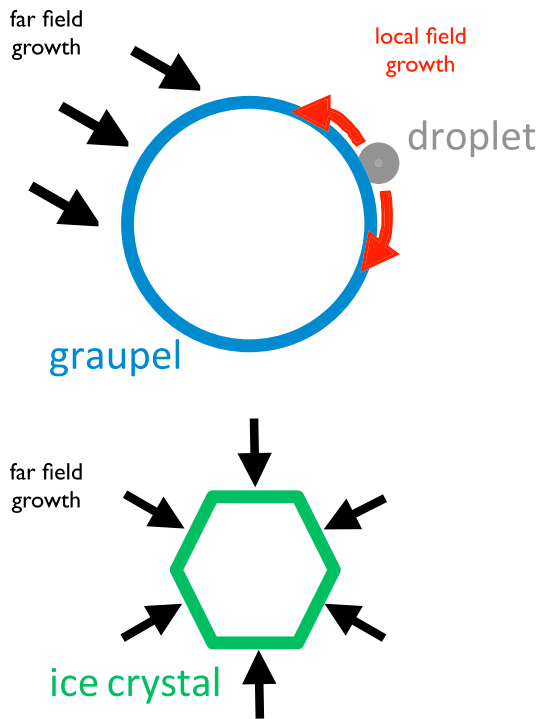


Figure 1. Illustration of the relative diffusional growth rate theory. The graupel particle (blue circle) grows by diffusion of water vapor from the far field (black arrows) as well as from the local field (red arrows) that is created by cloud droplets (gray circle) that partially evaporate while freezing onto the graupel surface during riming. Ice crystals (green hexagon) only grow from the far field.

of graupel particles, ice crystals, and cloud droplets. Laboratory results are typically presented as a functions of temperature and EW or LWC weighted with collision efficiency and relative fall velocity (rime accretion rate). Modeling studies have explored supersaturation (Mitzeva et al., 2005; Tsenova et al., 2010), ice and graupel radii, and relative fall velocities of graupel and ice particles as important parameters of the RDGR theory.

In this paper, we want to follow up on these theoretical studies by presenting a sensitivity study with a more realistic setting. We extend the RDGR theory to account for nonspherical particles and anisotropic diffusional growth, and we use numerical simulations to generate a realistic sampling of the RDGR parameter space rather than varying one parameter at a time as previous studies have done.

2. Methods

Our implementation of the RDGR theory follows Tsenova et al. (2009) with slight improvements (C. Saunders, and R. P. Mitzeva, personal communication, November/December 2014). Note that we do not consider the terminal fall velocity as an independent parameter but calculate it based on the hydrometeor size. We adapt the growth rates to account for nonspherical hydrometeors and anisotropic diffusional growth.

2.1. RDGR Theory for Nonspherical Hydrometeors

Nonsphericity affects the mass-size relationship $m = m(r)$, where r denotes the hydrometeor radius, or dominant length scale, needed for the conversion of mass into radius growth rates (terms $\partial r / \partial m$ in equation (3)). We follow Seifert and Beheng (2006) in assuming power law relationships

$$r_i = \frac{a_i}{2} \cdot m_i^{b_i} \text{ and } r_g = \frac{a_g}{2} \cdot m_g^{b_g}, \quad (4)$$

where the first equation with index i describes ice crystals and the second with index g graupel particles. We use parameter values $a_i = 0.835$, $a_g = 0.142$, $b_i = 0.390$, and $b_g = 0.314$ (Glassmeier & Lohmann, 2016).

The capacitance C accounts for the anisotropy of diffusional mass growth (terms $\partial m / \partial t$ in equation (3)) due to a nonspherical hydrometeor geometry. Typical ice crystal geometries corresponds to capacitances (Pruppacher & Klett, 2010)

$$C_i = c_i \cdot r_i, \quad (5)$$

where the geometry-dependent prefactor is given by

$$c_i = \begin{cases} 1 & \text{for spheres,} \\ \frac{2}{\pi} & \text{for thin hexagonal plates,} \\ \frac{\epsilon}{\arcsin(\epsilon)}, & \epsilon = \sqrt{1 - a^2} \text{ for oblates spheroids with axis lengths } r_1 = r_2 = r_i, r_3 = ar_i, \\ \frac{\epsilon}{\ln\left(\frac{1+\epsilon}{a}\right)}, & \epsilon = \sqrt{1 - a^2} \text{ for prolate spheroids with axis lengths } r_1 = r_i, r_2 = r_3 = ar_i. \end{cases} \quad (6)$$

The capacitance of the graupel particle can be assumed to result from its inhomogeneous surface properties caused by riming rather than as a result of a pronounced overall nonsphericity in shape. We assume that these surface effects can be lumped into a prefactor c_g such that equation (5) is also applicable to graupel.

Combining equations (3)–(5), the sign of graupel charge is determined by

$$\text{SoC} = \text{sign} \left[c_g \left(\frac{a_g b_g}{2} m^{b_g-1} \right) \left(\frac{dm_g}{dt} \right)_{\text{spherical}} - c_i \left(\frac{a_i b_i}{2} m^{b_i-1} \right) \left(\frac{dm_i}{dt} \right)_{\text{spherical}} \right] \quad (7)$$

$$= \text{sign} \left[c_a \left(\frac{a_g b_g}{2} m^{b_g-1} \right) \left(\frac{dm_g}{dt} \right)_{\text{spherical}} - \left(\frac{a_i b_i}{2} m^{b_i-1} \right) \left(\frac{dm_i}{dt} \right)_{\text{spherical}} \right], \quad (8)$$

where the capacitance prefactors of graupel and ice crystals can be lumped into a general anisotropy factor $c_a = c_g/c_i$ because $c_i > 0$ and thus does not change the sign of Δ upon division. The detailed expressions for the spherical mass growth rates are summarized in Appendix A.

2.2. Simulations

The sign of graupel charge predicted by the RDGR theory as formulated here depends on the following parameters: pressure, temperature, supersaturation, LWC, cloud droplet, ice crystal, and graupel size. We obtain sets of these parameters that are representative of in-cloud values from an idealized simulation of a thundercloud following Weisman and Klemp (1982) with a boundary-layer water vapor mixing ratio of 14 g/kg and a unidirectional vertical wind shear of 10 m/s between ground level and 6-km height. We apply the nonhydrostatic limited-area model of the Consortium for Small-scale Modeling (COSMO) (Baldauf et al., 2011; Vogel et al., 2009) in a high-resolution setup with a horizontal grid spacing of 500 m, a stretched vertical grid with 100 levels and a time step of 3 s. The extent of the model domain comprises 300×250 grid points in the directions parallel and perpendicular to the horizontal winds and 22 km in the vertical direction.

The model is coupled to a two-moment bulk microphysics scheme that predicts mass and number densities of six hydrometeor classes, that is, cloud droplets and rain drops, cloud ice, snow, graupel, and hail (Noppel et al., 2010; Seifert & Beheng, 2006). Equivalent particle radii are diagnosed from equation (4) by using the mean particle mass obtained from the ratio of particle mass and number densities. The microphysics scheme describes the partitioning between water vapor and liquid water based on a saturation adjustment approach such that saturation with respect to water is assumed whenever liquid is present. Mixed-phase regions as they are relevant for the RDGR theory thus always feature water.

The droplet activation follows the parameterization of Segal and Khain (2006) with a continental aerosol background. Primary ice nucleation follows Paukert and Hoose (2014) with dust-aerosol-dependent freezing of cloud droplets (immersion freezing). We perform simulations with dust number concentrations of 10^4 , 10^5 , 10^6 , 10^7 , and 10^8 m^{-3} in the lower atmosphere. The number concentration of cloud condensation nuclei (CCN) remains unchanged. Following the climatology of mineral dust over Europe (Hande et al., 2015), dust number concentration exponentially decays above 2 km. Dust aerosol is advected by the grid-scale circulation and diffused by subgrid turbulence. Ice multiplication by rime splintering follows Hallett and Mossop (1974).

3. Results

Figure 2 illustrates the thermodynamic and microphysical state of the simulated thundercloud 2.5 hr after convection was triggered in the conditionally unstable atmosphere of the Weisman and Klemp (1982) profiles by the release of a warm bubble. We base our analysis on this time step, because it corresponds to the mature stage of the storm and thus provides sufficient cloudy grid points for statistically robust results. As the microphysical state of the convective core quickly reaches a relatively steady state, our results are not particularly sensitive to the time step chosen for analysis. We present our analysis for the highest dust concentration because this concentration clearly results in a charge reversal line from positive to negative graupel charging with decreasing temperature that is approximately located in the expected temperature window (Williams, 1989) of -10 to -20°C . Sensitivities to the background aerosol are discussed in section 3.2.2. The RDGR theory can be applied to the mixed-phase region of a cloud when graupel is present. We define this region such that LWC, ice water content, and graupel water content all have to exceed minimal values of 10^{-10} kg/m^3 .

3.1. Anisotropy of Hydrometeors

Figure 3 illustrates the sign of graupel charging diagnosed from the simulation output for different choices of the anisotropy parameter c_a as a function of temperature and EW. The other four parameters, that is, the radii

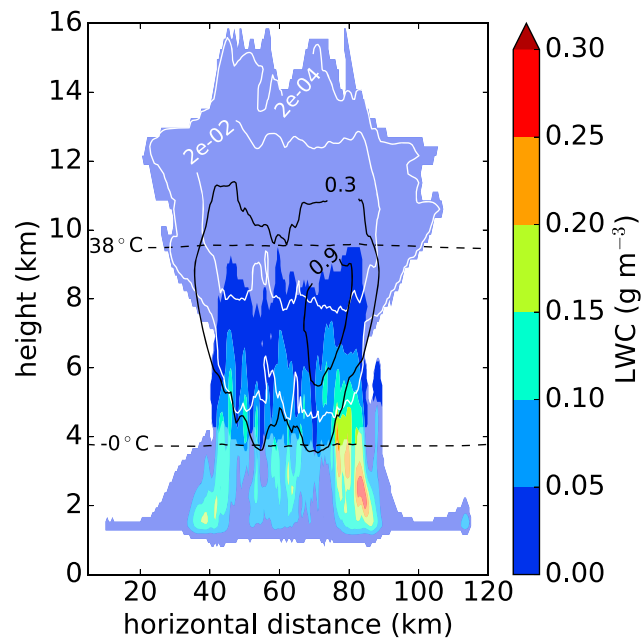


Figure 2. Horizontal average of liquid water content (filled contours), ice water content (white contours, in grams per cubic meter), graupel water content (dark gray contours, in grams per cubic meter), and temperature (black dashed contour lines) at $t = 2.5$ hr in the simulated cloud for a dust concentration of 10^{-8} m^{-3} . The mixed-phase region, which is relevant for the relative diffusional growth rate theory, is highlighted by brighter colors. The color scale matches these saturated colors but also applies to the corresponding colors of lower saturation.

of ice crystals, graupel particles and droplets, and the pressure, are not controlled for, such that different signs of charge can occur for a given combination of temperature and EW. In lightly colored regions 20% to 50% of data points deviate from the majority charging sign. The approximate location of charge reversal lines can be inferred from the locations of dark-colored regions, where only 20% of data points deviate from the majority charging sign. The continuous transformation of these regions with changing values of the anisotropy parameter give additional guidance on where charge reversal lines are expected.

For isotropic hydrometeor growth ($c_a = 1$), we generally diagnose negative graupel charging everywhere in the simulated cloud (Figure 3), while the positive charge transfer to graupel particles dominates for a strong anisotropic growth as illustrated for $c_a = 8$. Such strong anisotropies are probably not realistic because they would, for example, require a prolate ice crystals with $a = 0.1$ and very rough graupel with $c_g \approx 2.7$. For an intermediate value of $c_a = 3$, we obtain a distinct structure of charge transfer reversal lines. To obtain the expected charge transfer reversal from the RDGR theory in combination with realistic parameter combinations, we thus find it necessary to use c_a as a tuning parameter similar to the use of the ventilation coefficient in Mitzeva et al. (2005). Concerning its interpretation, it is important to note that the charging pattern is also highly sensitive to the particle geometry given by the a and b parameters in equation (7). In our study, we keep fixed values of a and b but changing their values would have a similar (although in the case of b nonlinear) effect as changing the anisotropy parameter c_a . The anisotropy parameter can thus be interpreted as encompassing both, the uncertainties of the anisotropy of diffusional growth, represented by capacitances, as well as the anisotropy of the resulting particle geometry, represented by $r(m)$ and its derivative. In this sense, the tuning parameter c_a accounts for processes acting on the microscale that are not represented by a bulk cloud microphysics scheme but that are important for the RDGR theory. We choose a tuning of $c_a = 3$ for the rest of our analysis because the corresponding pattern includes a charge reversal line from positive to negative graupel charging with decreasing temperature that is approximately located in the expected temperature window (Williams, 1989) of -10 to -20°C .

The charging structure in Figure 3 (c) can be separated into two regimes, which will be discussed in the remainder of this section. For the first regime with $\text{EW} < 0.6 \text{ g/m}^3$, charge transfer reversal lines are approximately vertical, which means that the sign of the charge transfer is mainly determined by temperature and largely

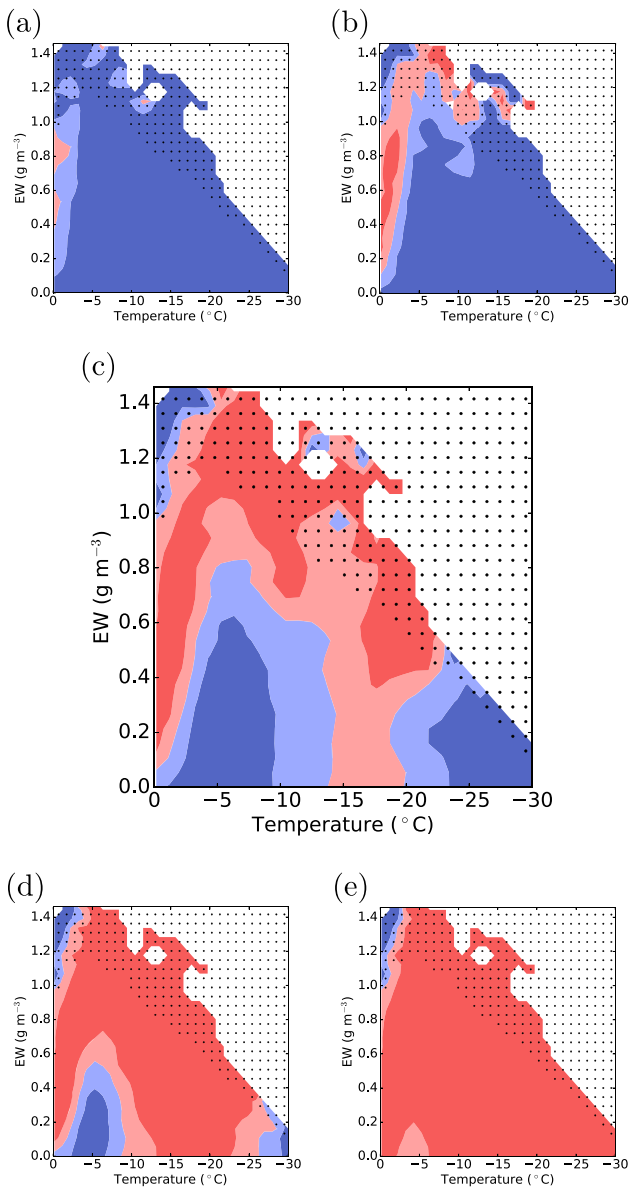


Figure 3. Regions of positive (red) and negative (blue) graupel charging as a function of temperature and effective water content (EW) in the simulated cloud for hydrometeor anisotropies of (a–e) $c_a = 1, 2, 3, 4, 8$. This study focuses on the case in (c), $c_a = 3$, which is shown enlarged. Colors correspond to the majority charging of data points in the bin. Dark colors indicate regions where <20% of data points differ in charging from the majority charging. Stipplings indicate a sample size <30 for the bin average.

independent of EW. For the second regime with $EW > 0.6 \text{ g/m}^3$, the charge transfer reversal line is more horizontal, indicating a dependence of charging on EW.

3.2. Temperature, Cloud Microphysics, and Ice Crystal Radius

The dependence of the SoC transfer on temperature in the $EW < 0.6 \text{ g/m}^3$ regime can be traced back to being mediated by the ice crystal radius r_i . Figure 4 shows that the temperature dependence vanishes when controlling for r_i instead of EW. The SoC appears to vary with temperature because the ice crystal radius is a function of the temperature in the cloud as illustrated in Figure 5 (top). The maximum of the ice crystal radius at about -15°C corresponds to a minimum in the diffusional radius growth rate of the ice crystals (Figure 5, bottom, blue line) because diffusional radius growth rates—in contrast to mass growth rates—are inversely proportional to the hydrometeor radius. The growth rate of the ice crystal is thus smaller than that of the graupel particle (Figure 5, bottom, black line). This explains the region of positive graupel charging between -14 and -20°C in Figure 3c. Graupel charges negatively below and above this region.

3.2.1. Susceptibility Analysis

Our observation that the SoC is controlled by the ice crystal radius for $EW < 0.6 \text{ g/m}^3$ is consistent with the sensitivities of the RDGR theory to its different input parameters with the ice crystal radius being the dominant one. We quantify these in the form of relative sensitivities, or susceptibilities,

$$s(p, T, LWC, r_c, r_i, r_g) = \frac{\partial \ln \Delta(p, T, LWC, r_c, r_i, r_g)}{\partial \ln X} = \frac{\frac{1}{\Delta} \partial \Delta(p, T, LWC, r_c, r_i, r_g)}{\frac{1}{X} \partial X} \quad (9)$$

that is, as normalized or logarithmic partial derivatives of the diffusional growth rate difference Δ to the input parameters $X \in \{p, T, LWC, r_c, r_i, r_g\}$. The use of the term *susceptibility* is motivated by the *albedo susceptibility*, defined by Platnick and Twomey (1994), and *precipitation susceptibility*, subsequently introduced by Feingold and Siebert (2009). Like their electric and magnetic counterparts, susceptibilities have the advantage over non-relative sensitivities that they are dimensionless such that they can directly be compared for different input parameters.

We use automatic differentiation to derive the partial derivatives from our implementation of the RDGR theory as described in Appendix A. Automatic differentiation is a computational technique that needs to be distinguished from both numerical and symbolic differentiation. Instead, the source code of the function to be derived—which may contain iterative elements—is decomposed into elemental computations like addition and exponentiation. By repeated application of the chain rule, this decomposition then allows construction of the derivative based on the known symbolic derivatives of the limited number of elemental functions. Practically, programming language-specific software packages for automatic differentiation are available (aut, 2018, <http://www.autodiff.org/>). For our

python code, we use the package `autograd` (Maclaurin et al., 2017). The automatic differentiation routine provided by `autograd` takes our python routine for the RDGR as input and provides a new routine as output, which is an implementation of the derivative of our RDGR routine. We stress that only source code is required to obtain the derivative routine. Simulation output is not needed.

The derivatives $s(p, T, LWC, r_c, r_i, r_g)$ are functions of all the input parameters such that their evaluation requires a sampling of the parameters space in the same manner as $\Delta(p, T, LWC, r_c, r_i, r_g)$ does. Figure 6 shows the susceptibilities resulting from our in-cloud sampling of the parameter space. The figure shows that the ice crystal radius is indeed the dominant RDGR parameter except for $EW > 0.6 \text{ g/m}^3$, where the local growth becomes important. This high EW regime will be discussed in the next section. The susceptibility to the ice

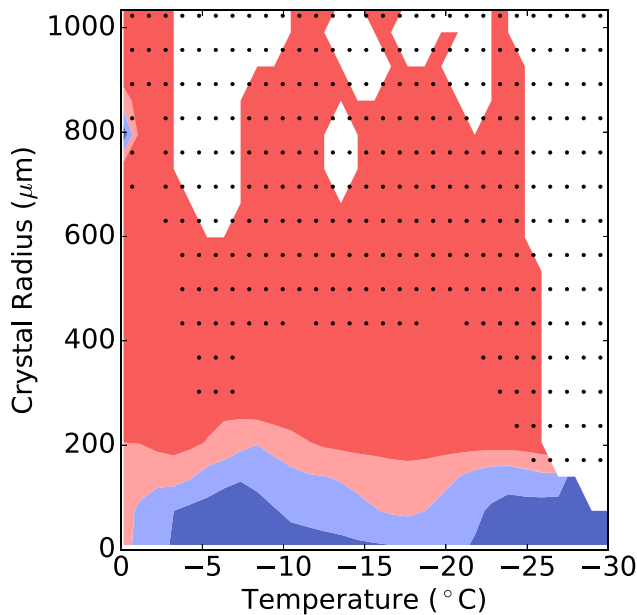


Figure 4. Regions of positive (red) and negative (blue) graupel charging as a function of temperature and ice radius for all data points in the simulated cloud for a hydrometeor anisotropy of $c_a = 3$. Colors correspond to the majority charging of data points in the bin. Dark colors indicate regions where <20% of data points differ in charging from the majority charging. Stipplings indicate a sample size <30.

crystal radius is closely followed by that to the graupel radius. This is in accordance with Tsenova et al. (2009), who found the ice crystal radius to be more important than the graupel radius for EW below 1 g/m^3 and temperatures above -7°C .

3.2.2. Cloud Microphysics and Aerosol Effects

The temperature profile of the crystal radius (Figure 5, top) is the result of temperature-dependent cloud microphysical processes, in particular ice multiplication and heterogeneous freezing (Figure 7). Ice multiplication following Hallett and Mossop (1974) is a significant source of large numbers of small ice crystals at warm temperatures, which explains the small ice crystal radii found in this regime. The negative graupel charging at in the lower part of the simulated cloud is thus the result of ice multiplication.

While being transported upward in the updraft, ice crystals grow by diffusion until their size peaks around -15°C . At colder temperatures, the heterogeneous freezing of cloud droplets adds new, small ice crystals to the population such that the mean ice crystal size is reduced.

The hypothesis that temperature controls cloud microphysical processes, which in turn determine the ice crystal radius, and thus, the SoC transfer is confirmed when perturbing the cloud microphysical state of the simulated cloud. To perturb the sizes of ice and graupel, we vary the concentration of dust aerosol while keeping the number concentration of CCN constant. Dust aerosol acts as ice nucleating particles in our simulations such that increased dust concentrations enhance heterogeneous freezing. Ice multi-

plication is not directly affected by the concentration of ice nucleating particles. Figure 8 (top) in fact illustrates that lower dust concentrations result in larger ice crystals at cold temperatures, while the ice crystal radii at

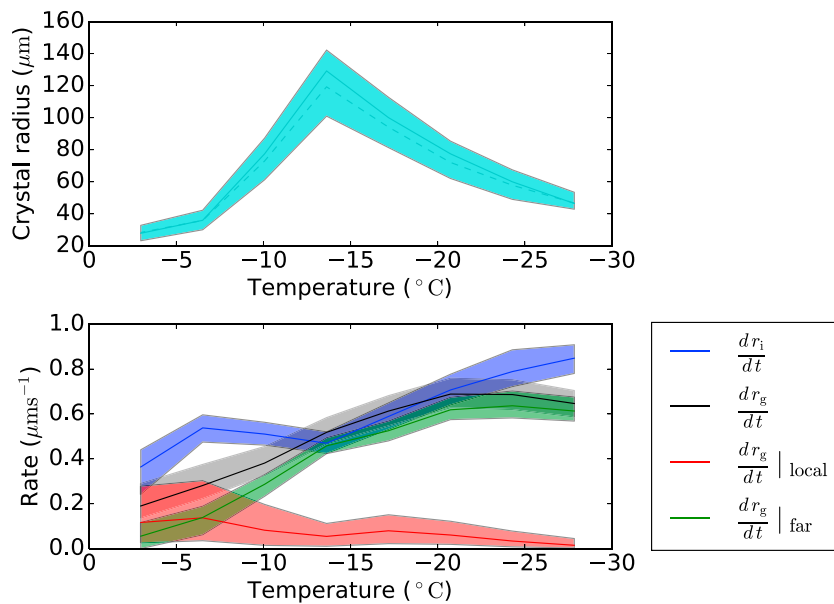


Figure 5. Ice crystal radius (top, cyan) in the simulated cloud and resulting rates of ice radius growth (bottom, blue) and total graupel radius growth (bottom, black) for $c_a = 3$ with its contributions from the local (bottom, red) and far (bottom, green) field as a function of cloud temperature. Solid lines are median values over all data points in the simulated cloud with the colored shading indicating the 20th and 80th percentiles. The cyan dashed line in the top plot shows the ice radius of the most frequent combination of ice and graupel radii for a given temperature as obtained from the maximum of a 2-D histogram of ice and graupel radii (it is this ice radius, rather than the median, that is reflected in the growth rates, which are calculated from combinations of ice and graupel radii.).

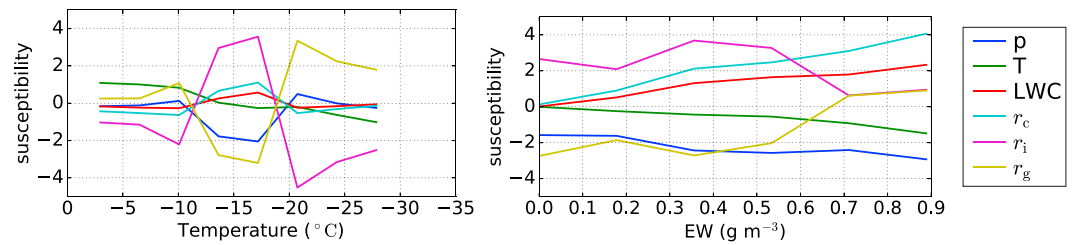


Figure 6. Median susceptibilities of the diffusional growth rate difference $\Delta = dr_g/dt - dr_i/dt$ to pressure (blue), ambient temperature (green), liquid water content (red), cloud droplet radius (cyan), ice crystal radius (magenta), and graupel radius (yellow) as a function of (left) temperature and (right) effective water content as sampled by the simulated in-cloud values.

warm temperatures are unaffected. The corresponding aerosol effect on the SoC transfer is shown in Figure 8 (bottom). It causes an extension of the positive charging region to temperatures $T < -20$ °C.

What we discuss here, is the primary effect of aerosol via hydrometeor size on the SoC separation. This effect cannot be studied with current charge-separation parameterizations that only depend on EW and temperature and not on hydrometeor sizes. The direct effect has to be distinguished from secondary effects of microphysical perturbations. As described by Zhao et al. (2015), a CCN perturbation can lead to an increase in cloud water content that changes the sign of graupel charging according to an EW- and T -dependent parameterization. Mansell and Ziegler (2013) discuss that CCN perturbations also affect graupel-ice crystal collision rates and thus the total charge separation.

3.3. EW and Growth From the Local Field

The LWC influences the RDGR via the local growth of the graupel particle (equations (3) and (A2)). Figure 5 (bottom) illustrates that this local contribution to the overall graupel growth rate is largest for temperatures $T > -10$ °C. This is the temperature regime, however, where ice multiplication quickly reduces the bulk average ice crystal size (section 3.2). Small ice crystal radii lead to ice crystal radius growth rates that are larger than the graupel radius growth rates, even including the local vapor field. In our simulation, the effect of the local field is therefore masked by the fast radius growth rate of the numerous, small ice crystals resulting from ice multiplication.

Our simulation samples the EW- T parameter space reliably for a wide range of temperatures for values of $EW < 0.6$ g/m³. Figure 5 is therefore dominated by and most representative for regions with $EW < 0.6$ g/m³. Higher EW are only well sampled for temperatures $T > -12$ °C. Restricting the analysis to warm temperatures, Figure 9 shows that vapor deposition from the local field dominates overall graupel growth almost for the whole EW range (for $EW > 0.1$ g/m³). At $EW > 0.7$ g/m³, the graupel depositional growth rate, which is entirely due to the local field, becomes larger than the ice crystal growth rate. The EW dependence of Figure 3c at $T > -12$ °C can thus be attributed to the local contribution of the graupel growth rate.

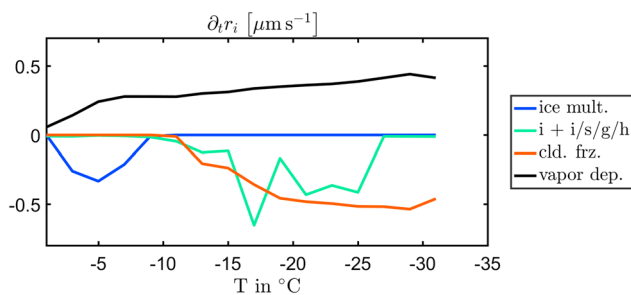


Figure 7. Bulk average radius growth rates of the ice crystals from ice multiplication (blue), aggregation of ice-phase hydrometeors (green), heterogeneous freezing of cloud droplets (orange), and vapor deposition (black) versus temperature for all data points in the simulated cloud. Note that the vapor deposition rate deviates slightly from the one in Figure 5 because the plot is based on direct model output (mean values) instead of offline diagnosed rates (median values).

The dominance of the local growth for $EW > 0.7$ g/m³ also changes the importance of susceptibilities of the RDGR theory to its parameters. As shown in Figure 6 (right), the growth rate difference is most susceptible to the cloud droplet radius and pressure and least susceptible to the sizes of graupel and ice for $EW > 0.6$ g/m³. The strong sensitivity to the cloud droplet radius follows because the graupel growth equation from the local vapor field is directly proportional to it (equation (A2)). The sensitivity to the pressure is probably related to its effect on the graupel ventilation coefficients via the air density (sections A1 and A2). A strong sensitivity of the RDGR theory to ventilation has been discussed by Mitzeva et al. (2005).

3.4. Implications for Laboratory Results

The weak sensitivity of the RDGR to crystal and graupel size in the local-growth dominated regime is in accordance with laboratory studies of Jayaratne et al. (1983) and Keith and Saunders (1990), which do not find a crystal size dependence of the SoC. Both studies report $LWC \approx 1$ g/m³,

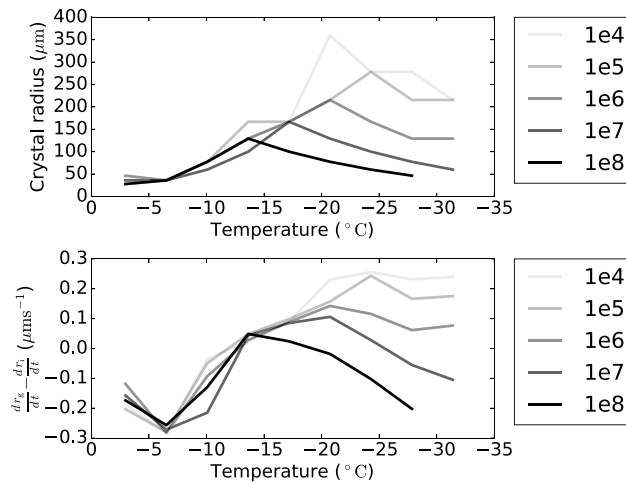


Figure 8. Ice crystal radius (top) and relative diffusional growth rate (bottom) for $c_d = 3$ as a function of temperature in the simulated cloud for dust concentrations from 10^4 to 10^8 m^{-3} as indicated. Note that the black lines in this figure directly correspond to Figure 5.

which Keith and Saunders (1990) relate to $EW \approx 0.5 \text{ g/m}^3$. This seems reasonably close to the onset of a significant contribution from local growth to the RDGR in Figure 9.

An alternative explanation for the absence of a crystal size dependence may be related to the nonsphericity of ice crystals, which is not controlled for in the experiments. Both studies grow their ice crystals naturally, which results in ice crystal habits and ice densities that vary with temperature. In equation (7), this temperature-dependent nonsphericity corresponds to a temperature-dependent capacitance $c_i(T)$ and to temperature-dependent parameters $\alpha_i(T)$, $\beta_i(T)$. The temperature dependence of these parameters may mask the size dependence of the RDGR. Ice crystal habits may thus provide an alternative to ice crystal size in explaining the temperature dependence of the SoC based on the RDGR theory.

In accordance with the susceptibilities from Figure 6, the ice crystal radius dependence of the RDGR dominates over the effect of EW, except for $EW > 0.7 \text{ g/m}^3$ and $T < -12^\circ \text{C}$. As illustrated in Figure 10, EW generally controls the SoC when the dominant variability of the ice crystal radius is removed by fixing its value. This observation is very interesting in the context of laboratory studies as sketched in Figure 10. The *one-chamber* study of Saunders and Peck (1998) corresponds to a well-mixed mixed-phase situation at water saturation and reports a horizontal charge reversal line, similar to our results for fixed ice crystal radius. *Two-chamber* studies by Takahashi (1978),¹ Saunders et al. (2006), and Pereyra et al. (2000) are performed during the equilibration phase after mixing cloud droplet- and ice crystal-containing air masses, which corresponds to ice crystals and graupel particles experiencing supersaturations that deviate from water saturation. These studies find more vertical charge reversal lines, similar to our results for variable ice crystal radius.

Considering their curvature and positive-to-negative (with decreasing temperature) charge reversal, the observed charge reversal lines best correspond to the charge reversal line at -20°C in this study. We

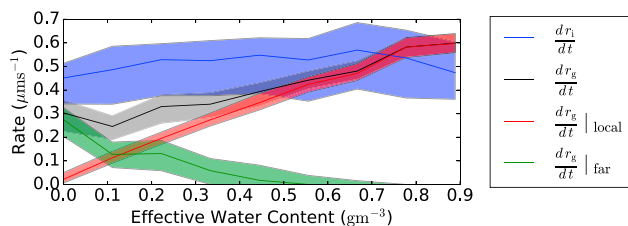


Figure 9. Same as Figure 5 (bottom), but for effective water content instead of temperature and a restricted temperature range of $0^\circ \text{C} > T > -12^\circ \text{C}$.

simulate a deep storm (Figure 2), and Stolzenburg et al. (1998b) observe an upward shift of the expected charge-sign-reversal region to colder temperatures with increasing storm depth. It therefore is plausible that we observe a charge reversal line at the lower end of the expected temperature range.

Our study shows a region of negative graupel charging at $T > -15^\circ \text{C}$ and $EW < 0.7 \text{ g/m}^3$. As discussed, this region is the result of ice multiplication. The deviation of the model derived signs of charge and laboratory results, which also have successfully been applied in simulating observed storms,

¹ According to Saunders et al. (2006) this study can be considered two-chamber like although it was performed with a single chamber.

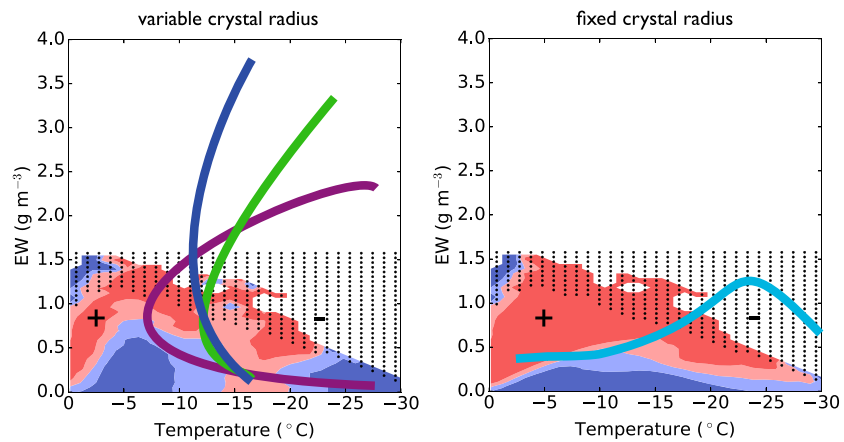


Figure 10. Regions of positive (red) and negative (blue) graupel charging as a function of temperature and EW for (a) values in the simulated cloud (same as Figure 3c) and (b) values in the simulated cloud but with a fixed ice crystal radius $r_i = 80 \mu\text{m}$ for $c_a = 3$. Colors correspond to the majority charging of data points in the bin. Dark colors indicate regions where $<20\%$ of data points differ in charging from the majority charging. Stipplings indicate a sample size <30 . Lines sketch the charge reversal lines obtained from laboratory results of Takahashi (1978; purple), Saunders et al. (2006; dark blue), Pereyra et al. (2000; green), and Saunders and Peck (1998; light blue). EW = effective water content.

can on the one hand be explained by the fact that simulations of mixed-phase cloud microphysics remain difficult. On the other hand, one should bear in mind that we simulate an idealized storm that may be atypical.

Saunders et al. (2014) suggests that the differences in supersaturation can explain the differently shaped charge reversal lines between one- and two-chamber experiments. Given that the ice crystal size is reasonably well constrained in one-chamber experiments and probably less constrained in two-chamber experiments, our results in Figure 10 offer an alternative explanation for the experimentally observed differences. The differences are probably the result of a combination of an ice crystal radius and supersaturation effect. To answer this question—under the assumption that the RDGR theory explains charge separation—new laboratory results that measure the ice crystal radius as a function of temperature are required.

4. Conclusion

We have presented a follow-up analysis to the theoretical sensitivity studies of Mitzeva et al. (2005) and Tsenova et al. (2009) that explores the RDGR theory in a more realistic setting. On the one hand we account for nonspherical particles and anisotropic diffusional growth, and on the other hand we use numerical simulations of an idealized thundercloud to obtain a sampling of the RDGR parameter space that is representative for in-cloud values.

We find that nonsphericity and anisotropy strongly shift the relative strength of ice crystal and graupel growth rates and thus control the extent of regions of positive graupel charging (Figure 3). We introduce a single tuning parameter (equation (7)) that encapsulates the combined effect of microscopic hydrometeor properties, that is, shape and growth characteristics, that are parameterized in typical cloud-microphysics schemes.

Our numerical in-cloud sampling of the parameter space enables us to relate the pattern of charging regions and charge reversal lines as predicted by the RDGR theory to cloud microphysics. We identify two regimes. The largest part of the mixed-phase region of the thundercloud features $\text{EW} < 1 \text{ g m}^{-3}$. In this regime, the local growth of graupel can be neglected and the sign of the graupel charge is controlled by the ice crystal radius as the dominant parameter (Figure 6). The ice crystal radius varies as a function of in-cloud temperature in our results (Figure 5). It peaks at an intermediate temperature of $T \approx -15^\circ\text{C}$ because the mean ice crystal radius is reduced by ice multiplication for high temperature ($T > -15^\circ\text{C}$), and by heterogeneous freezing of cloud droplets at temperatures $T < -15^\circ\text{C}$ (Figure 7). This relationship between temperature, cloud microphysics, and the ice crystal radius explains the charge transfer reversal with temperature according to the RDGR theory. Variations in the concentration of ice nucleating particles modulate the ice crystal radius at colder temperatures and can thus influence the charging pattern. We find that the extent of the region of positive graupel charging increases for lower INP concentrations and corresponding larger ice crystals. In light of evidence for lightning enhancement under polluted aerosol conditions (Altartatz et al., 2017, and ref-

erences therein; Thornton et al., 2017), it would be very interesting to investigate the role such primary effects of aerosol on charge separation in comparison to secondary effects like changes in the location and extent of the mixed-phase region.

The graupel growth from the local field crucially controls the sign of graupel charge at effective water contents $EW > 0.6 \text{ g/m}^3$, which are restricted to temperatures $T > -12^\circ \text{C}$ in our simulations (Figure 9). In contrast to laboratory studies, we find a region of negative graupel charging for $T > -14^\circ \text{C}$ and $EW < 0.6$. In this region, the effect of ice multiplication on ice crystal size and the corresponding large growth rates of ice crystals mask the contribution from the local field (Figure 5).

For this study, we have assumed that the anisotropy parameter c_a (equation (7)) is a constant and does in particular not depend on the temperature T . The habit of ice crystals is strongly influenced by temperature (e.g., Lohmann et al., 2016). Here we concentrated on an assumed effect of riming on the anisotropy of graupel, which explains our choice. A T -dependent anisotropy parameter $c_a(T)$ may contribute to the observed T dependence of the SoC in addition or alternatively to a T dependence of the ice crystal size. Our discussion in the following largely applies to both scenarios, T -dependent ice crystal size and T -dependent ice crystal habit.

In this study, we considered a six-dimensional parameter space for the RDGR theory that is spanned by pressure, temperature, LWC, and the radii of cloud droplets, ice crystals, and graupel particles. Laboratory results are typically reported in a two-dimensional reduction of the six-dimensional space, namely, as a function of temperature and EW only. This raises the question, if a two-dimensional representation is at all appropriate and which two variables best capture the sensitivities of the RDGR theory. For the far-field dominated regime, our susceptibility analysis shows that the ice crystal radius followed by the graupel radius are the most dominant parameters of the RDGR theory (Figure 6). This result is in accordance with the weaker statement of Tsenova et al. (2009) that the ice crystal radius is more important than the graupel radius except for warm temperatures and very high water contents ($EW > 1 \text{ g/m}^3$). For the regime dominated by the local field, the RDGR is most sensitive to cloud droplet radius and pressure (Figure 6). Based on these susceptibilities, a T -EW representation of laboratory results seems neither optimal for the local nor the far-field dominated regime. In particular, we find that the T -EW representation hides the importance of the ice crystal radius (or potentially the ice crystal habit) and might complicate the comparison and interpretation of laboratory studies (Figure 10). As a further implication, the experimental radius (along with the habit) needs to vary with temperature in a way representative of in situ in-cloud values to make laboratory results reported in the T -EW space applicable for usage in numerical models. Given that most numerical models used for electrification studies feature two-moment microphysics schemes today and thus predict ice crystal radii, it seems unnecessary to parameterize the effect of the ice crystal radius via temperature within the RDGR theory. Due to the regime-dependent sensitivities, a two-dimensional representation of RDGR results in general seems difficult. Instead, charge separation according to the RDGR theory could be explicitly represented in models. The use of two-moment cloud microphysics schemes allows for the prediction of crucial parameters of the RDGR theory as bulk averages while hydrometeor anisotropy could be handled by the tuning parameter introduced here, potentially in a temperature-dependent version $c_a(T)$.

The above discussions assume that the RDGR theory is indeed the correct model behind collisional charge separation. The fact that the T -EW representation does not seem consistent with the RDGR theory but has proven successful in reporting laboratory studies and for parameterizations points to potential problems with the RDGR theory. Our results specifically suggest that the laboratory studies of Jayaratne et al. (1983) and Keith and Saunders (1990) should be extended to test if the SoC depends on ice crystal and graupel sizes for a range of EW and when controlling for the ice crystal habit. If the RDGR theory is the correct model, such a relationship is expected from our results. New laboratory studies that control the ice crystal radius as a function of temperature along with hydrometeor properties and growth anisotropy would be desirable. Those would allow to quantitatively, instead of qualitatively as, for example, Emersic and Saunders (2010), test the RDGR theory.

Even given the theoretical feasibility of an explicit parameterization of charge separation according to the RDGR theory, the sensitivity of the RDGR theory to certain parameters poses a challenge for numerical models. In this study, we found the SoC to critically depend on the ice crystal radius, which in our case is shaped by ice multiplication and heterogeneous freezing. Both processes are still poorly understood (Field et al., 2016; Kanji et al., 2017), and their parameterizations in models are extremely uncertain. If our model took high-temperature ice nucleating particles, for example, from biological material (Hoose & Möhler, 2012; Kanji

et al., 2017) into account, the onset of heterogeneous freezing would be shifted to warmer temperatures, as would the maximum of the ice crystal radius. This could shift the positive-to-negative charge reversal currently located at -20°C —which may be appropriate for a supercell storm (Stolzenburg et al., 1998b)—to a more typical position around -15°C . Similarly, ice multiplication parameterizations beyond (Hallett & Mossop, 1974), for example, by ice-ice collisions (Yano & Phillips, 2011), which are active at colder temperatures are expected to modify the pattern of the charging regions. As a third example, an aerosol-aware freezing of rain drops as recently suggested by Paukert et al. (2017) is expected to affect the crystal radius-temperature relationship: As the majority of potential ice nuclei is converted to rain-sized drops due to collision and coalescence, more cloud water is available for riming at high altitudes. In turn, the sensitivity to aerosol concentrations results from the freezing probabilities of rain, and the altitude of maximum ice radii is determined by ice crystal conversion due to riming.

As far as uncertainties in hydrometeor shape and density, that is, mass-size relationships, are concerned, new approaches to modeling mixed-phase cloud microphysics that replace the distinction between ice crystals, snowflakes, and graupel particles by an adaptive ice-phase category of process-dependent density (Morrison & Milbrandt, 2015) seem promising. In terms of crystal habit and graupel anisotropy, approaches like Jensen et al. (2017), which take specific growth axis into account to describe anisotropic diffusional growth of ice-phase hydrometeors could replace the tuning parameter c_a . Last but not least, the numerical simulations in this study are based on assuming water saturation in mixed-phase regions. Modeling studies based on predicted supersaturation report supersaturations as high as 10% to 15% with respect to liquid water in convective updrafts, especially in pristine aerosol conditions (Grabowski & Morrison, 2017; Lebo et al., 2012). This indicates that the assumption of water saturation might be problematic, especially given the reported strong sensitivities of the RDGR theory to supersaturation (Mitzeva et al., 2005).

Laboratory experiments indicate a role of cloud water in the charge separation process. The RDGR theory in its current form explains the relevance of cloud water by the local contribution to graupel growth. Our study raises the questions if this is indeed the case. Next to the indirect effect of the local growth on the far-field growth via an increased graupel surface temperature (equation (A1)), effects of cloud droplets on far-field ventilation along the lines of Mitzeva et al. (2005) offer an alternative explanation. Our study suggests that also an effect of the riming rate on the growth anisotropy of the graupel could mediate an influence of cloud water on charge separation without including local graupel growth.

In conclusion, charge generation in general and charge separation according to the RDGR theory and its microphysical controls in particular continue to pose a challenge from the microscale to the cloud scale. This study suggests that a combined effort of experimentalists and cloud microphysicists is required to clarify the role of the RDGR theory.

Appendix A

The following equations for the diffusional mass growth rates of spherical hydrometeors are based on Tsenova et al. (2009) as well as Pruppacher and Klett (2010) and Wallace and Hobbs (2006).

A1. Diffusional Mass Growth Rate of Spherical Graupel From the Far Field

$$\frac{dm_g}{dt} = F_f 4\pi r_g D_v [\rho_w(T_a) - \rho_i(T_g)] \quad (\text{A1})$$

r_g : spherical graupel radius

D_v : diffusion coefficient of water vapor in air (Pruppacher & Klett, 2010)

$\rho_w(T_a)$: saturation vapor density with respect to water at in-cloud temperature T_a

T_a : (ambient) cloud temperature

$\rho_i(T_g)$: saturation vapor density with respect to ice at graupel surface temperature T_g

T_g : temperature of graupel surface; following (Macklin & Payne, 1967) it is determined by

$$EW \cdot V \cdot \frac{L_f + c_w(T_a - T_0) + c_i(T_0 - T_g)}{4} = \chi \cdot \text{Re}^{\frac{1}{2}} \cdot \frac{\text{Pr}^{\frac{1}{3}} K(T_g - T_a) + \text{Sc}^{\frac{1}{3}} D_v L_s [\rho_i(T_g) - \rho_a(T_a)]}{2r_g}$$

EW: effective water content; $EW = \text{LWC} \cdot E_{\text{coll}}$

LWC: liquid water content

$$E_{\text{coll}} = E_g \cdot E_c \text{ (Seifert \& Beheng, 2006)}$$

$$E_g = \begin{cases} 0 & \text{if } 2r_g \leq 150\mu\text{m} \\ 1 & \text{if } 2r_g > 150\mu\text{m} \end{cases}$$

$$E_c = \begin{cases} 0 & \text{if } 2r_d < 10\mu\text{m} \\ \frac{2r_d - 10\mu\text{m}}{30\mu\text{m}} & \text{if } 10\mu\text{m} \leq 2r_d \leq 40\mu\text{m} \\ 1 & \text{if } 2r_d > 40\mu\text{m} \end{cases}$$

L_f : latent heat of freezing; $L_f = 0.333 \cdot 10^6$ J/kg

L_s : latent heat of sublimation; $L_s = 2.834 \cdot 10^6$ J/kg (Seifert & Beheng, 2006)

c_w : specific heat of liquid water; $c_w = 4,187$ J/kg/K

T_0 : melting temperature of ice; $T_0 = 273.15$ K

K : thermal conductivity (see Lohmann et al., 2016, p. 191)

Pr : Prandtl number; $Pr = \frac{c_p \gamma_a \sigma_a}{K}$

c_p : specific heat of dry air at constant pressure; $c_p = 1,005$ J/kg/K

χ : numerical factor, adapted for spherical particles from Avila et al. (1999) according to Tsenova et al. (2009);

$$\chi = 0.6 + 0.83 \exp(-5.17 \cdot 10^{17} \cdot r_d^4 \cdot V)$$

c_i : specific heat of ice; $c_i = 2,093.4$ J/kg/K (Rogers & Yau, 1989)

F_f : ventilation coefficient for the far vapor field of the graupel (Pruppacher & Klett, 2010)

$$F_f = \begin{cases} 1 + 0.108(\text{Sc}^{\frac{1}{3}} \text{Re}^{\frac{1}{2}})^2 & \text{if } \text{Sc}^{\frac{1}{3}} \text{Re}^{\frac{1}{2}} < 1.4 \\ 0.78 + 0.308(\text{Sc}^{\frac{1}{3}} \text{Re}^{\frac{1}{2}}) & \text{if } \text{Sc}^{\frac{1}{3}} \text{Re}^{\frac{1}{2}} \geq 1.4 \end{cases}$$

Sc : Schmidt number; $Sc = \frac{\gamma_a}{D_v}$

Re : Reynolds number; $Re = \frac{2r_g V}{\gamma_a}$

V : graupel terminal velocity (Mansell et al., 2010), (Wisner et al 1972)

$$V = \left(\frac{\sigma_{a0}}{\sigma_a} \cdot \frac{4\sigma_g g}{3c_d \sigma_a} \cdot 2r_g \right)^{\frac{1}{2}}$$

σ_g : graupel density

C_d : drag coefficient; $C_d = 0.8$

g : gravitational acceleration; $g = 9.8$ m/s²

σ_{a0} : air density at the surface, $\sigma_{a0} \approx 1.225$ kg/m³ (Seifert & Beheng, 2006)

σ_a : air density; $\sigma_a = \frac{p}{R_d T_a (1 + 0.608 q_v)}$

p : pressure

q_v : specific humidity

R_d : specific gas constant of dry air; $R_d = 287$ J/kg/K (Pruppacher & Klett, 2010)

γ_a : kinematic viscosity of air; $\gamma_a \approx 1.4086 \cdot 10^{-5}$ m²/s (Seifert & Beheng, 2006)

A2. Diffusional Mass Growth Rate of Spherical Graupel From the Local Vapor Field

$$\frac{dm_g}{dt} = 3F_l D_v r_d 2^{\frac{1}{3}} [\rho_w(T_0) - \rho_l(T_g)] \cdot \frac{6r_g^2 \cdot V \cdot EW}{4\sigma_w r_d^3} \cdot \tau_f \quad (\text{A2})$$

F_l : ventilation coefficient for the local vapor field of the graupel; $F_l = \chi \cdot \text{Re}^{0.6} \cdot \text{Pr}^{\frac{1}{3}}$

σ_w : water density

τ_f : freezing time of cloud droplets on the graupel surface, given by the implicit relationship below that requires numerical solving (Tsenova et al. (2009) with modifications from C. Saunders and R. P. Mitzeva, personal communications, November/December 2014

$$0 = 2\pi r_d \{L_s D_v F_l [\rho_w(T_0) - \rho_w(T_a)] + F_l K(T_0 - T_a)\} \tau_f + (T_0 - T_g) K_i r_d^2 \sqrt{\frac{\pi}{K_i}} \tau_f - \left\{ \frac{2\pi}{3} r_d^3 \sigma_w [L_f - c_w(T_0 - T_a)] \right\} \quad (A3)$$

K_i : heat conductivity of ice (~ 250 K, $\sim 1,013$ hPa); $K_i = 2.4$ W/m/K (Slack, 1980)

A3. Diffusional Mass Growth Rate of Spherical Ice Crystals

$$\frac{dm_i}{dt} = F_c \frac{4\pi r_i (S_i - 1)}{\frac{L_s}{KR_v T_a^2} + \frac{R_v T_a}{e_i D_v}} \quad (A4)$$

F_c : ventilation coefficient for the ice crystal; following Tsenova et al. (2009), we assume $F_c = 1$

r_i : ice crystal radius

S_i : saturation ratio with respect to ice; the model applied here features a saturation adjustment with respect to water, that is, $S_i = \frac{e_w}{e_i}$

e_i : saturation vapor pressure with respect to ice

e_w : saturation vapor pressure with respect to water

R_v : specific gas constant of water vapor; $R_v = 461.5$ J/kg/K (Pruppacher & Klett, 2010)

Acknowledgments

The authors thank Boryana Tsenova, Rumjana Miteva, and Clive Saunders for clarifying details of their RDGR calculations. We also thank Yoav Yair and two anonymous reviewers, whose comments were very helpful to improve this manuscript. Bernhard Vogel and Max Bangert are gratefully acknowledged for providing the COSMO-ART code that the model version used for this study was based on. M. P. was funded by the Helmholtz Association through the President's Initiative and Networking Fund (VH-NG-620). The simulation output is available at <http://hdl.handle.net/20.500.11850/268687>. The code of our python implementation of the RDGR theory is available at https://github.com/remodietlicher/rdgr_analysis.

References

- Altaratz, O., Kucienska, B., Kostinski, A., Raga, G. B., & Koren, I. (2017). Global association of aerosol with flash density of intense lightning. *Environmental Research Letters*, *12*, 114037.
- Avila, E. E., Castellano, N. E., & Saunders, P. R. (1999). Effects of cloud-droplet spectra on the average surface-temperature of ice accreted on fixed cylindrical collectors. *Quarterly Journal of the Royal Meteorological Society*, *125*, 1059–1074.
- Avila, E. E., Varela, G. G. A., & Caranti, G. M. (1995). Temperature dependence of static charging in ice growing by riming. *Journal of the Atmospheric Sciences*, *52*, 4515–4522. [https://doi.org/10.1175/1520-0469\(1995\)052<4515:TDOSCI>2.0.CO;2](https://doi.org/10.1175/1520-0469(1995)052<4515:TDOSCI>2.0.CO;2)
- Baker, B., Baker, M. B., Jayaratne, E. R., Latham, J., & Saunders, C. P. R. (1987). The influence of diffusional growth rates on the charge transfer accompanying rebounding collisions between ice crystals and soft hailstones. *Quarterly Journal of the Royal Meteorological Society*, *113*, 1193–1215. <https://doi.org/10.1002/qj.49711347807>
- Baker, M. B., & Dash, J. G. (1989). Charge transfer in thunderstorms and the surface melting of ice. *Journal of Crystal Growth*, *97*, 770–776.
- Baldauf, M., Seifert, A., Forstner, J., Majewski, D., & Raschendorfer, M. (2011). Operational convective-scale numerical weather prediction with the COSMO model: Description and sensitivities. *Monthly Weather Review*, *139*, 3887–3905. <https://doi.org/10.1175/MWR-D-10-05013.1>
- Barthe, C., Molinie, G., & Pinty, J.-P. (2005). Description and first results of an explicit electrical scheme in a 3D cloud resolving model. *Atmospheric Research*, *76*, 95–113.
- Brooks, I. M., & Saunders, C. P. R. (1994). An experimental investigation of the inductive mechanism of thunderstorm electrification. *Journal of Geophysical Research*, *99*(D5), 10,627–10,632.
- Buser, O., & Aufdermaur, A. N. (1977). Electrification by collisions of ice particles on ice or metal targets. In *Electrical Processes in Atmospheres Proceedings of the Fifth International Conference on Atmospheric Electricity* (pp. 294–301). Garmisch-Partenkirchen, Germany, 2–7 September 1974.
- Caranti, G. M., Avila, E. E., & Ré, M. A. (1991). Charge transfer during individual collisions in ice growing from vapor deposition. *Journal of Geophysical Research*, *96*(D8), 15,365–15,375. <https://doi.org/10.1029/90JD02691>
- Caranti, J. M., & Illingworth, A. J. (1980). Surface potentials of ice and thunderstorm charge separation. *Nature*, *284*, 44–46. <https://doi.org/10.1038/284044a0>
- Christian, H., Holmes, C. R., Bullock, J. W., Gaskell, W., Illingworth, A. J., & Latham, J. (1980). Airborne and ground-based studies of thunderstorms in the vicinity of Langmuir Laboratory. *Quarterly Journal of the Royal Meteorological Society*, *106*, 159–174. <https://doi.org/10.1002/qj.49710644711>
- Dash, J. G., Mason, B. L., & Wettlaufer, J. S. (2001). Theory of charge and mass transfer in ice-ice collisions. *Journal of Geophysical Research*, *106*(D17), 20,395–20,402.
- Dash, J. G., & Wettlaufer, J. S. (2003). The surface physics of ice in thunderstorms. *Canadian Journal of Physics*, *81*, 201–207. <https://doi.org/10.1139/P03-011>
- Dinger, J. E., & Gunn, R. (1946). Electrical effects associated with a change of state of water. *Terrestrial Magnetism and Atmospheric Electricity*, *51*, 477–494. <https://doi.org/10.1029/TE051i004p00477>
- Emersic, C., & Saunders, C. (2010). Further laboratory investigations into the relative diffusional growth rate theory of thunderstorm electrification. *Atmospheric Research*, *98*(2–4), 327–340. <https://doi.org/10.1016/j.atmosres.2010.07.011>
- Feingold, G., & Siebert, H. (2009). Cloud-aerosol interactions from the micro to the cloud scale. In J. Heintzenberg & R. J. Charlson (Eds.), *Clouds in the perturbed climate system, Strüngmann Forum Reports* (pp. 597). Cambridge, MA: MIT Press.
- Field, P. R., Lawson, R. P., Brown, P. R. A., Lloyd, G., Westbrook, C., Moiseev, D., et al. (2016). *Secondary ice production—Current state of the science and recommendations for the future, Meteorological Monographs*. Boston: American Meteorological Society. <https://doi.org/10.1175/amsmonographs-d-16-0014.1>
- Gaskell, W. (1981). A laboratory study of the inductive theory of thunderstorm electrification. *Quarterly Journal of the Royal Meteorological Society*, *107*, 955–966. <https://doi.org/10.1002/qj.49710745413>
- Gaskell, W., & Illingworth, A. J. (1980). Charge transfer accompanying individual collisions between ice particles and its role in thunderstorm electrification. *Quarterly Journal of the Royal Meteorological Society*, *106*, 841–854. <https://doi.org/10.1002/qj.49710645013>
- Glassmeier, F., & Lohmann, U. (2016). Constraining precipitation susceptibility of warm, ice- and mixed-phase clouds with microphysical equations. *Journal of the Atmospheric Sciences*, *73*(12), 5003–5023. <https://doi.org/10.1175/JAS-D-16-0008.1>

- Grabowski, W. W., & Morrison, H. (2017). Modeling condensation in deep convection. *Journal of the Atmospheric Sciences*, *74*, 2247–2267. <https://doi.org/10.1175/jas-d-16-0255.1>
- Hallett, J., & Mossop, S. C. (1974). Production of secondary ice particles during the riming. *Nature*, *249*, 26–28.
- Hande, L. B., Engler, C., Hoose, C., & Tegen, I. (2015). Seasonal variability of Saharan desert dust and ice nucleating particles over Europe. *Atmospheric Chemistry and Physics*, *15*, 4389–4397. <https://doi.org/10.5194/acp-15-4389-2015>
- Helsdon, J. H., Wojcik, W. A., & Farley, R. D. (2001). An examination of thunderstorm-charging mechanisms using a two-dimensional storm electrification model. *Journal of Geophysical Research*, *106*(D1), 1165–1192.
- Hoose, C., & Möhler, O. (2012). Heterogeneous ice nucleation on atmospheric aerosols: A review of results from laboratory experiments. *Atmospheric Chemistry and Physics*, *12*(20), 9817–9854. <https://doi.org/10.5194/acp-12-9817-2012>
- Jayaratne, E. R. (1991). Charge separation during the impact of sand on ice and its relevance to theories of thunderstorm electrification. *Atmospheric Research*, *26*, 407–424. [https://doi.org/10.1016/0169-8095\(91\)90061-Z](https://doi.org/10.1016/0169-8095(91)90061-Z)
- Jayaratne, E. R. (1993). Temperature gradients in ice as a charge generation process in thunderstorms. *Atmospheric Research*, *29*, 247–260. [https://doi.org/10.1016/0169-8095\(93\)90006-A](https://doi.org/10.1016/0169-8095(93)90006-A)
- Jayaratne, E. R., Saunders, C. P. R., & Hallett, J. (1983). Laboratory studies of the charging of soft-hail during ice crystal interactions. *Quarterly Journal of the Royal Meteorological Society*, *109*, 609–630.
- Jensen, A. A., Harrington, J. Y., Morrison, H., & Milbrandt, J. A. (2017). Predicting ice shape evolution in a bulk microphysics model. *Journal of the Atmospheric Sciences*, *74*(6), 2081–2104. <https://doi.org/10.1175/jas-d-16-0350.1>
- Jungwirth, P., Rosenfeld, D., & Buch, V. (2005). A possible new molecular mechanism of thundercloud electrification. *Atmospheric Research*, *76*, 190–205. <https://doi.org/10.1016/j.atmosres.2004.11.016>
- Kanji, Z. A., Ladino, L. A., Wex, H., Boose, Y., Burkert-Kohn, M., Cziczko, D. J., & Krämer, M. (2017). Overview of ice nucleating particles. *Meteorological Monographs*, *58*, 1.1–1.33. <https://doi.org/10.1175/amsmonographs-d-16-0006.1>
- Keith, W. D., & Saunders, C. P. R. (1990). Further laboratory studies of the charging of graupel during ice crystal interactions. *Atmospheric Research*, *25*, 445–464.
- Kolomeychuk, R. J., McKay, D. C., & Iribarne, J. V. (1975). The fragmentation and electrification of freezing drops. *Journal of the Atmospheric Sciences*, *32*, 974–979. [https://doi.org/10.1175/1520-0469\(1975\)032<0974:TFAEOF>2.0.CO;2](https://doi.org/10.1175/1520-0469(1975)032<0974:TFAEOF>2.0.CO;2)
- Latham, J., & Dye, J. E. (1989). Calculations on the electrical development of a small thunderstorm. *Journal of Geophysical Research*, *94*(D11), 13,141–13,144.
- Latham, J., & Mason, B. J. (1961a). Electric charge transfer associated with temperature gradients in ice. *Proceedings of the Royal Society of London Series A*, *260*, 523–536. <https://doi.org/10.1098/rspa.1961.0051>
- Latham, J., & Mason, B. J. (1961b). Generation of electric charge associated with the formation of soft hail in thunderclouds. *Proceedings of the Royal Society of London Series A*, *260*, 537–549. <https://doi.org/10.1098/rspa.1961.0052>
- Latham, J., Petersen, W. A., Deierling, W., & Christian, H. J. (2007). Field identification of a unique globally dominant mechanism of thunderstorm electrification. *Quarterly Journal of the Royal Meteorological Society*, *133*(627), 1453–1457. <https://doi.org/10.1002/qj.133>
- Latham, J., & Warwicker, R. (1980). Charge transfer accompanying the splashing of supercooled raindrops on hailstones. *Quarterly Journal of the Royal Meteorological Society*, *106*, 559–568. <https://doi.org/10.1002/qj.49710644912>
- Lebo, Z. J., Morrison, H., & Seinfeld, J. H. (2012). Are simulated aerosol-induced effects on deep convective clouds strongly dependent on saturation adjustment? *Atmospheric Chemistry and Physics*, *12*(20), 9941–9964. <https://doi.org/10.5194/acp-12-9941-2012>
- Lohmann, U., Lüönd, F., & Mahr, F. (2016). *An introduction to clouds from microscale to climate*. Cambridge, UK: Cambridge University Press.
- Maclaurin, D., Duvenaud, D., & Johnson, M. (2017). Autograd—Software package for automatic differentiation in Python. <https://github.com/HIPS/autograd>.
- Macklin, W. C., & Payne, G. S. (1967). A theoretical study of the ice accretion process. *Quarterly Journal of the Royal Meteorological Society*, *93*(396), 195–213.
- Mansell, E. R., & Ziegler, C. L. (2013). Aerosol effects on simulated storm electrification and precipitation in a two-moment bulk microphysics model. *Journal of the Atmospheric Sciences*, *70*(7), 2032–2050. <https://doi.org/10.1175/jas-d-12-0264.1>
- Mansell, E. R., Ziegler, C. L., & Bruning, E. C. (2010). Simulated electrification of a small thunderstorm with two-moment bulk microphysics. *Journal of the Atmospheric Sciences*, *67*(1), 171–194. <https://doi.org/10.1175/2009jas2965.1>
- Marshall, B. J. P., Latham, J., & Saunders, C. P. R. (1978). Laboratory study of charge transfer accompanying the collision of ice crystals with a simulated hailstone. *Quarterly Journal of the Royal Meteorological Society*, *104*, 163–178.
- Mason, B. J. (1953). A critical examination of theories of charge generation in thunderstorms. *Tellus*, *5*, 446–460. <https://doi.org/10.1111/j.2153-3490.1953.tb01075.x>
- Mason, B. L., & Dash, J. G. (2000). Charge and mass transfer in ice-ice collisions: Experimental observations of a mechanism in thunderstorm electrification. *Journal of Geophysical Research*, *105*(D8), 10,185–10,192.
- Matthews, J. H., & Mason, B. J. (1964). Electrification produced by the rupture of large water drops in an electric field. *Quarterly Journal of the Royal Meteorological Society*, *90*, 275–286. <https://doi.org/10.1002/qj.49709038506>
- Mitzeva, R., Saunders, C., & Tsenova, B. (2005). A modelling study of the effect of cloud saturation and particle growth rates on charge transfer in thunderstorm electrification. *Atmospheric Research*, *76*(1-4), 206–221. <https://doi.org/10.1016/j.atmosres.2004.11.019>
- Morrison, H., & Milbrandt, J. A. (2015). Parameterization of cloud microphysics based on the prediction of bulk ice particle properties. Part I: Scheme description and idealized tests. *Journal of the Atmospheric Sciences*, *72*(1), 287–311. <https://doi.org/10.1175/jas-d-14-0065.1>
- Noppel, H., Blahak, U., Seifert, A., & Beheng, K. D. (2010). Simulations of a hailstorm and the impact of CCN using an advanced two-moment cloud microphysical scheme. *Atmospheric Research*, *96*, 286–301. <https://doi.org/10.1016/j.atmosres.2009.09.008>
- Paukert, M., & Hoose, C. (2014). *Journal of Geophysical Research: Atmospheres*, *119*, 9073–9092. <https://doi.org/10.1002/2014JD021917>
- Paukert, M., Hoose, C., & Simmel, M. (2017). Redistribution of ice nuclei between cloud and rain droplets: Parameterization and application to deep convective clouds. *Journal of Advances in Modeling Earth Systems*, *9*, 514–535. <https://doi.org/10.1002/2016MS000841>
- Pereyra, R. G., Avila, E. E., & Castellano, N. E. (2000). A laboratory study of graupel charging. *Journal of Geophysical Research*, *105*(D16), 20,803–20,812.
- Platnick, S., & Twomey, S. (1994). Determining the susceptibility of cloud albedo to changes in droplet concentration with the advanced very high resolution radiometer. *Journal of Applied Meteorology and Climatology*, *33*, 334–347.
- Pruppacher, H. R., & Klett, J. D. (2010). *Microphysics of clouds and precipitation* (2nd ed.). Netherlands: Springer.
- Reinhart, B. (2014). Coauthors understanding the relationships between lightning, cloud microphysics, and airborne radar-derived storm structure during hurricane karl (2010). *Monthly Weather Review*, *142*(2), 590–605. <https://doi.org/10.1175/mwr-d-13-00008.1>
- Reynolds, S. E., Brook, M., & Foulks Gourley, M. (1957). Thunderstorm charge separation. *Journal of Atmospheric Sciences*, *14*, 426–436.
- Rogers, R. R., & Yau, M. K. (1989). *A short course in cloud physics*. Oxford, New York: Pergamon Press.

- Sartor, D. (1954). A laboratory investigation of collision efficiencies, coalescence and electrical charging of simulated cloud droplets. *Journal of Atmospheric Sciences*, *11*, 91–103. [https://doi.org/10.1175/1520-0469\(1954\)011<0091:ALIOCE>2.0.CO;2](https://doi.org/10.1175/1520-0469(1954)011<0091:ALIOCE>2.0.CO;2)
- Saunders, C. P. R., Bax-Norman, H., Emersic, C., Avila, E. E., & Castellano, N. E. (2006). Laboratory studies of the effect of cloud conditions on graupel/crystal charge transfer in thunderstorm electrification. *Quarterly Journal of the Royal Meteorological Society*, *132*(621), 2653–2673. <https://doi.org/10.1256/qj.05.218>
- Saunders, C. P. R., Keith, W. D., & Mitzeva, R. P. (1991). The effect of liquid water on thunderstorm charging. *Journal of Geophysical Research*, *96*(D6), 11,007–11,017.
- Saunders, C., Mitzeva, R., & Tsenova, B. (2014). Further analysis of the effects of supersaturation on graupel charging—Modeling study. XV International Conference on Atmospheric Electricity.
- Saunders, C. P. R., & Peck, S. L. (1998). Laboratory studies of the influence of the rime accretion rate on charge transfer during crystal/graupe collisions. *Journal of Geophysical Research*, *103*(D12), 13,949–13,956.
- Saunders, C. P. R., Peck, S. L., Varela, G. G. A., Avila, E. E., & Castellano, N. E. (2001). A laboratory study of the influence of water vapour and mixing on the charge transfer process during collisions between ice crystals and graupel. *Atmospheric Research*, *58*, 187–203.
- Scavuzzi, C. M., & Caranti, G. M. (1996). Thunderstorm electrification analysis: The dependence on the temperature-LWC diagram. *Journal of the Atmospheric Sciences*, *53*, 349–358.
- Segal, Y., & Khain, A. (2006). Dependence of droplet concentration on aerosol conditions in different cloud types: Application to droplet concentration parameterization of aerosol conditions. *Journal of Geophysical Research*, *111*, D15204. <https://doi.org/10.1029/2005JD006561>
- Seifert, A., & Beheng, K. D. (2006). A two-moment cloud microphysics parameterization for mixed-phase clouds. Part 1: Model description. *Meteorology and Atmospheric Physics*, *92*, 45–66. <https://doi.org/10.1007/s00703-005-0112-4>
- Simpson, G. C. (1909). On the electricity of rain and its origin in thunderstorms. *Philosophical Transactions of the Royal Society A*, *209*, 379–413. <https://doi.org/10.1098/rspa.1909.0020>
- Simpson, G. C. (1927). The mechanism of a thunderstorm. *Proceedings of the Royal Society of London Series A*, *114*, 376–401. <https://doi.org/10.1098/rspa.1927.0048>
- Slack, G. A. (1980). Thermal conductivity of ice. *Physical Review B*, *22*(6), 3065–3071.
- Stolzenburg, M., Rust, W. D., & Marshall, T. C. (1998b). Electrical structure in thunderstorm convective regions: 3. Synthesis. *Journal of Geophysical Research*, *103*(D12), 14,097–14,108.
- Stolzenburg, M., Rust, W. D., & Marshall, T. C. (1998a). Electrical structure in thunderstorm convective regions: 2. Isolated storms. *Journal of Geophysical Research*, *103*(D12), 14,079–14,096.
- Takahashi, T. (1978). Riming electrification as a charge generation mechanism in thunderstorms. *Journal of the Atmospheric Sciences*, *35*, 1536–1548.
- Takahashi, T., Tajiri, T., & Sonoi, Y. (1999). Charges on graupel and snow crystals and the electrical structure of winter thunderstorms. *Journal of Atmospheric Chemistry*, *56*, 1561–1578.
- Thornton, J. A., Virts, K. S., Holzworth, R. H., & Mitchell, T. P. (2017). Lightning enhancement over major oceanic shipping lanes. *Geophysical Research Letters*, *44*, 9102–9111. <https://doi.org/10.1002/2017GL074982>
- Tsenova, B., Mitzeva, R., & Saunders, C. (2009). A modelling study of the effect of ice particle sizes and relative velocity on ice crystal/graupe collisional charge transfer. *Atmospheric Research*, *91*, 250–258.
- Tsenova, B., Mitzeva, R., & Saunders, C. (2010). Parameterization of thunderstorm charging including the cloud saturation effect. *Atmospheric Research*, *96*(2-3), 356–365. <https://doi.org/10.1016/j.atmosres.2009.11.010>
- Vogel, B., Vogel, H., Bäumer, D., Bangert, M., Lundgren, K., Rinke, R., & Stanelle, T. (2009). The comprehensive model system COSMO-ART—Radiative impact of aerosol on the state of the atmosphere on the regional scale. *Atmospheric Chemistry and Physics*, *9*, 8661–8680. <https://doi.org/10.5194/acp-9-8661-2009>
- Wallace, J. M., & Hobbs, P. V. (2006). *Atmospheric science: An introductory survey* (2nd ed.). Amsterdam, Netherlands: Elsevier.
- Weisman, M. L., & Klemp, J. B. (1982). The dependence of numerically simulated convective storms on vertical wind shear and buoyancy. *Monthly Weather Review*, *110*.
- Williams, E. R. (1989). The tripole structure of thunderstorms. *Journal of Geophysical Research*, *94*(D11), 13,151–13,167.
- Williams, R. Z., Zhang, R., & Rydock, J. (1991). Mixed-phase microphysics and cloud electrification. *Journal of the Atmospheric Sciences*, *48*, 2195–2203. [https://doi.org/10.1175/1520-0469\(1991\)048<2195:MPMACE>2.0.CO;2](https://doi.org/10.1175/1520-0469(1991)048<2195:MPMACE>2.0.CO;2)
- Wilson, C. T. R. (1929). Some thundercloud problems. *Journal of The Franklin Institute*, *208*, 1–12. [https://doi.org/10.1016/S0016-0032\(29\)90935-2](https://doi.org/10.1016/S0016-0032(29)90935-2)
- Workman, E. J., & Reynolds, S. E. (1950). Electrical phenomena occurring during the freezing of dilute aqueous solutions and their possible relationship to thunderstorm electricity. *Physical Review*, *78*, 254–259. <https://doi.org/10.1103/PhysRev.78.254>
- Yano, J.-I., & Phillips, V. T. J. (2011). Ice–ice collisions: An ice multiplication process in atmospheric clouds. *Journal of the Atmospheric Sciences*, *68*(2), 322–333. <https://doi.org/10.1175/2010jas3607.1>
- Zhao, P., Yin, Y., & Xiao, H. (2015). The effects of aerosol on development of thunderstorm electrification: A numerical study. *Atmospheric Research*, *153*, 376–391.
- Zilch, L. W., Maze, J. T., Smith, J. W., Ewing, G. E., & Jarrold, M. F. (2008). Charge separation in the aerodynamic breakup of micrometer-sized water droplets. *Journal of Physical Chemistry A*, *112*, 13,352–13,363. <https://doi.org/10.1021/jp806995h>